Journal of Biomolecular NMR, **21:** 361–366, 2001.
KLUWER/ESCOM

CPMG sequences with enhanced sensitivity to chemical exchange

Chunyu Wang, Michael J. Grey & Arthur G. Palmer, III
Department of Biochemistry and Molecular Biophysics, Columbia University, 630 West 168th Street, New York, NY 10032, U.S.A.

Received 27 July 2001; Accepted 16 October 2001

Key words: BPTI, chemical exchange, CPMG, dynamics, relaxation

Abstract

Improved relaxation-compensated Carr–Purcell–Meiboom-Gill pulse sequences are reported for studying chemical exchange of backbone ^{15}N nuclei. In contrast to the original methods [J. P. Loria, M. Rance, and A. G. Palmer, *J. Am. Chem. Soc. 121*, 2331–2332 (1999)], phenomenological relaxation rate constants obtained using the new sequences do not contain contributions from ^{1}H-^{1}H dipole-dipole interactions. Consequently, detection and quantification of chemical exchange processes are facilitated because the relaxation rate constant in the limit of fast pulsing can be obtained independently from conventional ^{15}N spin relaxation measurements. The advantages of the experiments are demonstrated using basic pancreatic trypsin inhibitor.

Relaxation-compensated Carr–Purcell–Meiboom–Gill (CPMG) sequences (Loria et al., 1999a, b) have proven useful in characterizing dynamic events on μs to ms time scales in protein backbones (Millet et al., 2000) and sidechains (Mulder et al., 2001; Skrynnikov et al., 2001). In these methods, ^{13}C or ^{15}N heteronuclear multiplet components are manipulated to ensure that, in the absence of chemical exchange, the average effective phenomenological relaxation rate constant, $R_2(1/\tau_{cp})$, is rendered independent of the spacing between 180° pulses, τ_{cp}. The variation of $R_2(1/\tau_{cp})$ as a function of τ_{cp}, which is termed relaxation dispersion, then depends only on chemical exchange processes:

$$R_2\left(1/\tau_{cp}\right) = R_{20} + R_{ex}\left(1/\tau_{cp}\right) \quad (1)$$

in which R_{20} is the relaxation rate constant in the absence of exchange and is equal to the relaxation rate constant in the limit of fast pulsing, $R_2(1/\tau_{cp} \rightarrow \infty)$, and $R_{ex}(1/\tau_{cp})$ is the contribution to the relaxation decay from chemical exchange processes alone. For example, in the two-site fast exchange limit (Luz and Meiboom, 1963),

$$R_{ex}(1/\tau_{cp}) = (\Phi_{ex}/k_{ex})\left[1 - \frac{2\tanh(k_{ex}\tau_{cp}/2)}{k_{ex}\tau_{cp}}\right] \quad (2)$$

in which k_{ex} is the chemical exchange rate constant; $\Phi_{ex} = p_a p_b \Delta\omega^2$; p_a and p_b are the fractional populations of the two sites, A and B; and $\Delta\omega$ is the resonance frequency difference for spins in site A and site B. Values of R_{20}, k_{ex}, and Φ_{ex} are determined experimentally by fitting Equations 1 and 2 to relaxation dispersion data. Other theoretical expressions are necessary for exchange processes that are not in the fast exchange limit on the chemical shift time scale (Carver and Richards, 1972; Ishima and Torchia, 1999; Jen, 1978). All relaxation rate constants utilized herein are defined in Table 1.

In the original relaxation-compensated CPMG sequence developed for backbone ^{15}N spins in proteins (Loria et al., 1999a):

$$R_{20} = \frac{1}{2}\left(R_2^S + R_2^{IS}\right) \approx R_2^S + \frac{1}{2}R_1^I \quad (3)$$

in which R_2^S and R_2^{IS} are the transverse relaxation rate constants for in-phase and antiphase ^{15}N (= S) magnetization resulting from ^{1}H-^{15}N dipolar and ^{15}N chemical shift anisotropy (CSA) interactions in the absence of chemical exchange, respectively, and R_1^I

*To whom correspondence should be addressed. E-mail: agp6@columbia.edu

Table 1. Relaxation rate constants

Rate constant	Definition
$R_2(1/\tau_{cp})$	Apparent transverse relaxation rate constant for original relaxation compensated pulse sequences (Equation 1).
R_{20}	Apparent transverse relaxation rate, in the absence of chemical exchange, for original relaxation compensated pulse sequences (Equation 3).
$R_2^{rczz}(1/\tau_{cp})$	Apparent transverse relaxation rate for pulse sequences presented in Figures 1 and 2 (Equation 5).
R_{20}^{rczz}	Apparent transverse relaxation rate, in the absence of chemical exchange, for pulse sequences presented in Figures 1 and 2 (Equation 6).
$R_{ex}(1/\tau_{cp})$	Chemical exchange contribution to transverse relaxation, which is dependent on the spacing between refocusing pulses, $1/\tau_{cp}$ (Equation 2).
R_2^S	Transverse relaxation rate constant for in-phase heteronuclear magnetization in the absence of chemical exchange.
R_2^{IS}	Transverse relaxation rate constant for antiphase heteronuclear magnetization in the absence of exchange.
R_1^S	Longitudinal relaxation rate constant for heteronuclear magnetization.
R_1^I	Longitudinal relaxation rate constant for proton magnetization.
R_1^{IS}	Longitudinal relaxation rate constant for heteronuclear two spin order.
η_{xy}	Rate constant for ^{15}N CSA and ^{15}N-^{1}H dipole-dipole cross-correlated transverse relaxation.
η_z	Rate constant for ^{15}N CSA and ^{15}N-^{1}H dipole-dipole cross-correlated longitudinal relaxation.

is the longitudinal relaxation rate constant for the attached amide ^{1}H (= I) spin due to dipolar interactions with surrounding protons. The second equality assumes that values of the spectral density function, $J(\omega)$, at frequencies near the ^{1}H Larmor frequency are negligible in the macromolecular limit. If necessary, reduced spectral density mapping (Farrow et al., 1995) can be used to improve the approximation. As illustrated by Equations 1 and 2, $R_2(1/\tau_{cp}) \rightarrow R_{20}$ when $k_{ex}\tau_{cp} < 1$. Thus, obtaining accurate values for exchange parameters by curve-fitting experimental relaxation dispersion data requires that the smallest value of τ_{cp} utilized satisfy the condition $k_{ex}\tau_{cp} < 1$. This condition is difficult to achieve for processes with $k_{ex} > 2000\ s^{-1}$ and limits the range of applicability of the original relaxation-compensated CPMG experiments.

The restriction that $k_{ex}\tau_{cp} < 1$ can be relaxed if R_{20} is measured independently of the CPMG experiment. In this case, the shortest value of τ_{cp} only needs to satisfy $k_{ex}\tau_{cp} < 10$ because exchange parameters can be determined from the initial decay of $R_2(1/\tau_{cp}) - R_{20}$; thus, for values of $\tau_{cp} > 1$ ms, exchange processes with k_{ex} as large as $10^4\ s^{-1}$ can be characterized. R_2^S can be determined for ^{15}N spins using established ^{1}H-^{15}N dipole/^{15}N CSA relaxation interference experiments that either measure the transverse interference relaxation rate constant, η_{xy}, and assume a fixed ratio between R_2^S and η_{xy} (Fushman et al., 1998; Tjandra et al., 1996) or measure both η_{xy} and the longitudinal interference relaxation rate constant, η_z (Kroenke et al., 1998). Thus, R_{20} can be obtained provided that R_1^I is measured. In the approach adopted herein, rather than measuring R_1^I, a relaxation period for $2I_zS_z$ two-spin order is incorporated directly into relaxation-compensated CPMG pulse sequences using a modified version of the constant relaxation time approach previously described (Akke and Palmer, 1996).

Pulse sequences for relaxation-compensated CPMG experiments that incorporate a two-spin order relaxation period are shown in Figures 1 and 2. The pulse sequence of Figure 1a is derived from the original relaxation compensated experiment and is used for values of $\tau_{cp} < 10$ ms (Loria et al., 1999a). The pulse sequence of Figure 1b is derived from the self-compensated CPMG experiment and is used for values of $\tau_{cp} = m/J$ in which $m = 1$ (10.8 ms) or 2 (21.6 ms), where J is the one bond coupling between amide ^{1}H and ^{15}N (Millet et al., 2000). The pulse sequence in Figure 2 is a double Hahn echo sequence used for $\tau_{cp} = 6/J$ (64.8 ms). The relaxation period for two-spin order is placed after the t_1 frequency labeling period to ensure that R_1^I is the selective longitudinal relaxation rate constant (Cavanagh et al., 1996; Ishima et al., 1998). The signal intensity in these pulse sequences is described by

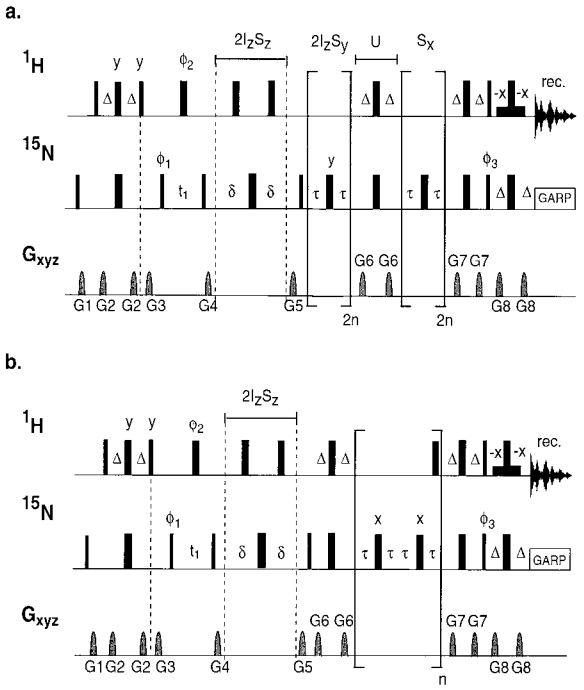

Figure 1. Pulse sequences for measuring ^{15}N $R_2^{rczz}(1/\tau_{cp})$ with (a) $\tau_{cp} < 10$ ms and (b) $\tau_{cp} = m/J$ with $m = 1$ (10.8 ms) or $m = 2$ (21.6 ms). The different strategies for averaging in-phase and antiphase ^{15}N magnetization in the two sequences have been discussed elsewhere (Millet et al., 2000). Narrow and wide bars depict 90° and 180° pulses, respectively, and short wide bars depict 1 ms water-selective 90° pulses. The 90° pulse lengths for proton and ^{15}N are approximately 10 μs at −1 dB and 40 μs at 0 dB, respectively. All pulses are x phase unless otherwise indicated. Delays are $\Delta = 2.7$ ms and $\tau = \tau_{cp}/2$. The total relaxation delay is (a) $t = 4n\tau_{cp}$ and (b) $t = 2n\tau_{cp}$, n is an integer, T is the maximum value of t, and $\delta = (T - t)/4$. ^{15}N decoupling was achieved with a 1.25 kHz GARP sequence (Shaka et al., 1985). The phase cycle is $\phi_1 = x, -x$; $\phi_2 = x, x, -x, -x$; $\phi_3 = 4$ (x), 4 (−x); and receiver = x, −x, x, −x, −x, x, −x. The gradients are sine shaped with durations G1-G8 = 2.0, 0.6, 2.0, 2.0, 1.0, 0.6, 0.6, 1.0 ms and amplitudes $G1_z = 4.4$, $G2_z = 3.0$, $G3_{xyz} = 12.0$, $G4_{xyz} = 9.0$, $G5_z = 4.5$, $G6_z = 3.0$, $G7_z = 3.0$, $G8_{xyz} = 9.0$ G/cm. Quadrature detection and axial peak suppression was achieved by phase cycling ϕ_1 and receiver using the States-TPPI scheme (Marion et al., 1989).

$$\begin{aligned} S(t) &= S(0)\exp\left[-R_1^{IS}(T-t)/2\right] \\ &\quad \exp\left[-R_2(1/\tau_{cp})t\right] \\ &= S(0)\exp\left[-R_1^{IS}T/2\right] \\ &\quad \exp\left[-\left(R_2(1/\tau_{cp}) - R_1^{IS}/2\right)t\right] \\ &= S'(0)\exp\left[-R_2^{rczz}(1/\tau_{cp})t\right] \end{aligned} \quad (4)$$

in which S(0) is the initial intensity after the t_1 period; R_1^{IS} is the relaxation rate constant for two spin order and $R_1^{IS} \approx R_1^I + R_1^S$ in the macromolecular limit, where R_1^S is the ^{15}N longitudinal relaxation rate constant; t is the total CPMG relaxation delay; T is the maximum value of t; and $S'(0) = S(0)\exp[-R_1^{IS}T/2]$ and

$$R_2^{rczz}(1/\tau_{cp}) = R_2(1/\tau_{cp}) - R_1^{IS}/2. \quad (5)$$

are the apparent initial intensity and relaxation rate constant in the new sequences, respectively. The apparent limiting relaxation rate constant is given by:

$$R_{20}^{rczz} = R_2^S - \frac{1}{2}R_1^S. \quad (6)$$

The limiting relaxation constant R_{20}^{rczz} is decreased compared with R_{20} (Equation 3), thereby making exchange term a larger proportion of the apparent rate constant and facilitating the detection of chemical exchange. More importantly, R_{20}^{rczz} can be determined independently of the CPMG experiments if R_2^S is measured as discussed above and R_1^S is measured using conventional experiments (Farrow et al., 1994). Finally, in the macromolecular limit, R_{20}^{rczz} is given by (Phan et al., 1996):

$$R_{20}^{rczz} = \frac{1}{6}\left(3d^2 + 4c^2\right)J(0) \quad (7)$$

in which d and c are the ^{1}H-^{15}N dipole and ^{15}N CSA coupling constants, respectively (Cavanagh et al., 1996). R_{20}^{rczz} scales with the static magnetic field strength simply due to the field dependence of c; therefore, R_{20}^{rczz} needs to be determined only at one field, either by curve-fitting to relaxation dispersion data or by independent measurements.

Although the relaxation rate constant for two-spin order could be measured in an independent experiment, rather than using the constant relaxation time approach, the proposed methods partially suppress the effects of multi-exponential relaxation of antiphase magnetization and two-spin order. Theoretical calculations similar to those employed by Kroenke and coworkers (1998), indicate that the pulse sequences of Figure 1 are compensated to first order in time and the pulse sequence of Figure 2 is compensated to second order in time. If desired, the pulse sequences in Figure 1 can be modified to yield second order compensation by adding a second relaxation period for two-spin order after the transverse relaxation period in a manner analogous to Figure 2.

The modified pulse sequences were validated using basic pancreatic trypsin inhibitor (BPTI); the chemical exchange process results from isomerization of the Cys 14 to Cys 38 disulfide bond in BPTI (Otting et al., 1993). All NMR experiments were performed on a 2.6 mM [U-98% ^{15}N] sample (Huang et al., 1997) at pH 5.1, 300 K using Bruker DRX600 and DRX500

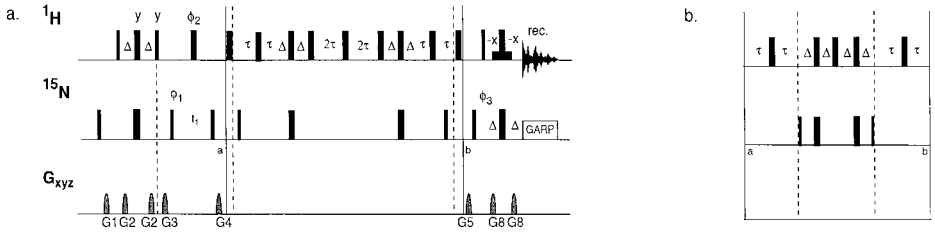

Figure 2. Double Hahn-echo sequence for $\tau_{cp} = 64.8$ ms. Only two time points were recorded to determine the relaxation rate constant. Data with a total relaxation delay t = 129.6 ms were acquired with the sequence in (a). Data with delay t = 0 were acquired by replacing the element between points a and b in (a) with the element in (b). The delay $\tau = \tau_{cp}/4 = 16.2$ ms. All other parameters are the same as for Figure 1.

spectrometers equipped with triple-resonance probes with three-axis gradients. Backbone assignments of BPTI were taken from Glushka et al. (1989). Two-dimensional (F1 × F2) spectra were acquired using (128 × 2048) complex points and spectral widths of (2000 × 10 000) Hz at 500 MHz and (2500 × 12500) Hz at 600 MHz. The recycle delay was 3 s and 16 transients were recorded for each complex point. At both 500 MHz and 600 MHz, τ_{cp} values of 1, 2, 6, 10 ms were employed for the sequence in Figure 1a, while τ_{cp} value of 10.8 and 21.6 ms were used for the sequence in Figure 1b at 600 MHz. A total of 10 to 12 relaxation time points (including duplicates) were acquired for each τ_{cp} value. At both 500 MHz and 600 MHz, 2 to 6 spectra were recorded using the pulse sequences of Figures 2a and 2b (τ_{cp} = 64.8 ms). Spectra were processed with nmrPipe (Delaglio et al., 1995). The t_1 dimension interferograms were apodized with a cosine-bell window function, zero filled by a factor of two and Fourier transformed. The t_2 dimension free induction decays were apodized with an exponential windows function with a line-broadening factor of 10 Hz, zero filled by a factor of two and Fourier transformed. Peak volumes were obtained using nlinLS (Delaglio et al., 1995). Data obtained using the pulse sequences in Figure 1 were fitted to a mono-exponential decay equation to obtain $R_2^{rczz}(1/\tau_{cp})$. Uncertainties in relaxation rates were determined by Monte Carlo simulation. For the pulse sequence of Figure 2, $R_2^{rczz}(1/\tau_{cp}) = \ln(S_b/S_a)/t$ in which S_a and S_b are the peak intensities obtained from Figures 2a and 2b, respectively. Uncertainties were obtained from duplicate measurements. R_1^S, R_2 (Farrow et al., 1994) and η_{xy} (Kroenke et al., 1998) were measured at both 500 MHz and 600 MHz by established methods. The conventional R_2 measurements used a 1 ms CPMG delay. The ratios $\kappa = R_2^S/\eta_{xy}$ (1.66 and 1.48 at 500 MHz and 600 MHz, respectively), were obtained as the average of R_2/η_{xy} for all residues in BPTI that are not subject to chemical exchange processes, assuming that the ^{15}N CSA is constant for all residues. For residues subject to chemical exchange, R_2^S was calculated as $\kappa\eta_{xy}$ and R_{20}^{rczz} was calculated from Equation 6. Variations in the ^{15}N CSA of 10 ppm (Kroenke et al., 1999) introduce <10% variation in R_{20}^{rczz} at 600 MHz.

The accuracy of the new experiments is illustrated using the results shown in Figures 3 and 4. The conventional R_2 experiment recorded with τ_{cp} = 1 ms yields the phenomenological rate constant $R_2 = R_2^S + R_{ex}(1/\tau_{cp} = 1\ ms^{-1})$ (Farrow et al., 1994; Palmer et al., 1992); thus, $R_2^{rczz}(1/\tau_{cp} = 1\ ms^{-1})$ is expected to be equal to $R_2 - R_1^S/2$. Figure 3a compares these data for 49 ^{15}N spins in BPTI at both 500 MHz and 600 MHz. Chemical exchange for Cys 38 in BPTI has $k_{ex}\tau_{cp} < 0.4$ for τ_{cp} = 1 ms and $R_2(1/\tau_{cp} \rightarrow \infty)$ is well-defined by curve-fitting $R_2(1/\tau_{cp})$ dispersion data obtained using the original relaxation-compensated pulse sequences (Millet et al., 2000). Figure 3b compares $R_2^{rczz}(1/\tau_{cp}) - R_{20}^{rczz}$ to $R_2(1/\tau_{cp}) - R_2(1/\tau_{cp} \rightarrow \infty)$ for Cys 38. Experimental $R_2(1/\tau_{cp})$ and fitted values of $R_2(1/\tau_{cp} \rightarrow \infty)$ were taken from Millet et al. (2000). Good linear correlations are obtained for both Figures 3a and 3b. Relaxation dispersion curves are depicted in Figure 4. Figure 4a shows $R_2^{rczz}(1/\tau_{cp}) - R_{20}^{rczz}$ relaxation dispersion data for the backbone amide ^{15}N spin of Cys 38 at both 500 MHz and 600 MHz. The existence of chemical exchange affecting Cys 38 is evident from the decay towards zero as $1/\tau_{cp}$ increases. Fitting of the dispersion data for Cys 38 yields exchange parameters $k_{ex} = 400 \pm 30\ s^{-1}$, $\Delta\omega = 460 \pm 14\ s^{-1}$, and $p_a = 0.951 \pm 0.002$ that are indistinguishable from the values of $k_{ex} = 380 \pm 70\ s^{-1}$, $\Delta\omega = 450 \pm 20\ s^{-1}$, and $p_a = 0.953 \pm 0.004$ obtained previously with the original relaxation-compensated CPMG pulse sequences (Millet et al., 2000). Figure 4b shows a typical flat $R_2^{rczz}(1/\tau_{cp})$ dispersion curve obtained for the back-

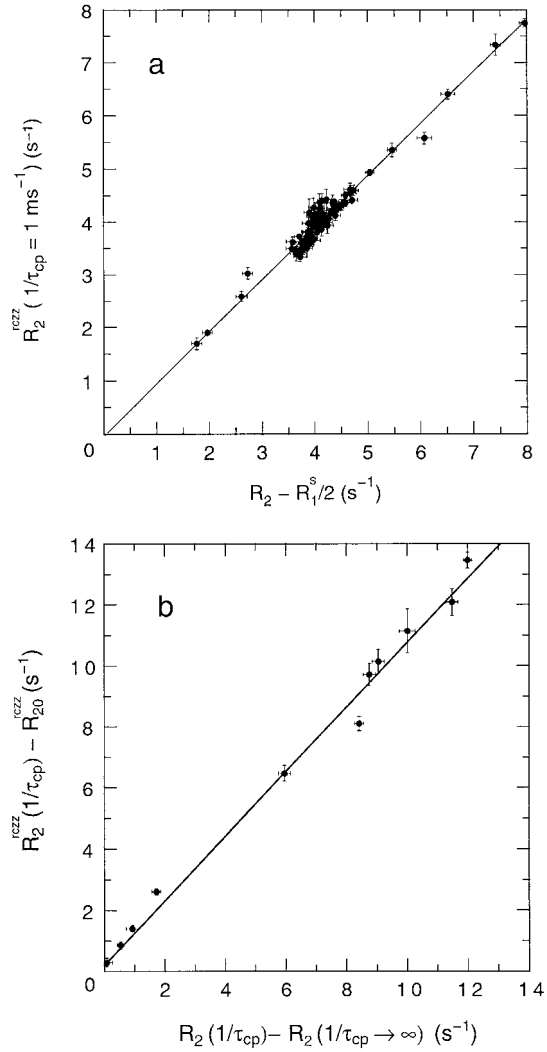

Figure 3. Accuracy of $R_2^{rczz}(1/\tau_{cp})$. (a) R_2^{rczz} ($1/\tau_{cp}$ = 1 ms^{-1}) acquired with the sequence in Figure 1a is plotted versus $R_2 - R_1^S/2$ for 49 spins in BPTI at 500 and 600 MHz. The optimal least squares line has a slope of 0.99 ± 0.02 and an intercept of −0.05 ± 0.08 s^{-1}. (b) $R_2^{rczz}(1/\tau_{cp}) - R_{20}^{rczz}$ obtained using the pulse sequences of Figures 1 and 2 and relaxation interference measurements is plotted versus $R_2(1/\tau_{cp}) - R_2(1/\tau_{cp} \rightarrow \infty)$ obtained from the original relaxation compensated methods and curve-fitting (Millet et al., 2000). The optimal least squares line has a slope of 1.04 ± 0.02 and an intercept of 0.4 ± 0.1 s^{-1}.

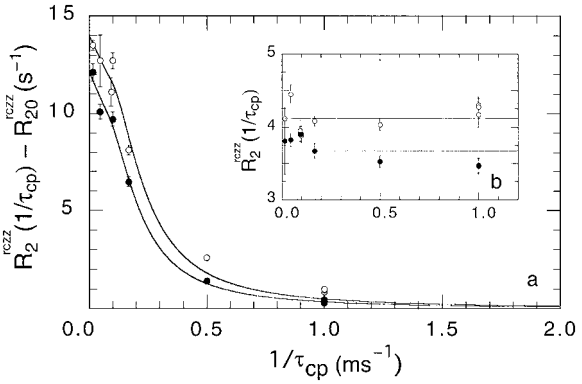

Figure 4. Relaxation dispersion for Gln 31 and Cys 38 in BPTI. (a) $R_2^{rczz}(1/\tau_{cp}) - R_{20}^{rczz}$ dispersion data for Cys 38 at (●) 500 MHz and (○) 600 MHz. The curves drawn in (a) are global fits using expressions for relaxation during CPMG sequences valid for all chemical exchange time scales; fits were performed as described elsewhere with the exception that the limiting values as $1/\tau_{cp} \rightarrow \infty$ were fixed at 0 (Millet et al., 2000). (b) $R_2^{rczz}(1/\tau_{cp})$ dispersion data for Gln 31, a residue not affected by chemical exchange. The lines drawn are the weighted mean of $R_2^{rczz}(1/\tau_{cp})$, 3.7 s^{-1} and 4.1 s^{-1}, at 500 MHz and 600 MHz, respectively. The standard deviation from the mean for both 500 and 600 MHz data are 0.2 s^{-1}. Values of R_{20}^{rczz} for Q31 are 3.8 ± 0.2 s^{-1} and 4.0 ± 0.2 s^{-1} at 500 and 600 MHz, respectively.

bone amide ^{15}N spin of Gln 31, a residue in BPTI that is not affected by chemical exchange processes. The average uncertainty in the relaxation rate constants for Gln 31 obtained in the new experiments are approximately 10% larger than the uncertainty obtained in the original experiments. Thus, although Equation 4 shows that the sensitivity of each two-dimensional experiment is reduced by a factor exp(–R_1^{IS}T/2), the final results obtained using the modified pulse sequences are of equally high quality as the original experiments.

The major advantage of the new pulse sequences is that R_{20}^{rczz} can be measured independently and is not an adjustable parameter obtained by fitting the relaxation dispersion data. This is especially useful when $k_{ex}\tau_{cp} > 1$ for the shortest value of τ_{cp} achievable experimentally, because fitting is possible even though the relaxation dispersion data will not approach the limiting value for $1/\tau_{cp} \rightarrow \infty$. As an illustration, the data in Figure 4a can be fit to yield $k_{ex} = 340 \pm 70$ s^{-1}, $\Delta\omega = 450 \pm 20$ s^{-1}, and $p_a = 0.948 \pm 0.005$ even if the data for $\tau_{cp} < 4$ ms is excluded, in which case $k_{ex}\tau_{cp} > 2$; such fitting is impossible if R_{20}^{rczz} must be included as an adjustable parameter, as in earlier approaches (Millet et al., 2000).

A second advantage of the new pulse sequences is that the difference $\Delta R_2 = R_2^{rczz}(1/\tau_{cp} = 15.4$ s$^{-1}) - R_{20}^{rczz}$ is a good approximation of the free-precession exchange rate constant, $R_{ex}(0)$, if exchange is fast or if $\Delta\omega > 100$ s^{-1} and $p_b/p_a < 0.15$. For the latter conditions, ΔR_2 differs from $R_{ex}(0)$ by <5% as calculated using expressions for $R_{ex}(1/\tau_{cp})$ given by Ishima and Torchia (1999). Thus, the chemical shift time scale for chemical exchange can be characterized using a scaling factor α^* defined as (Millet et al., 2000):

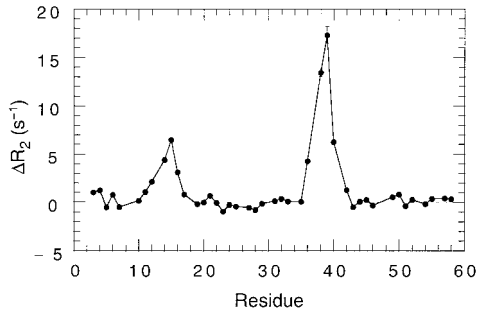

Figure 5. $\Delta R_2 = R_2^{rczz}(1/\tau_{cp} = 15.4\ s^{-1}) - R_{20}^{rczz}$ are plotted versus residue numbers in BPTI at 600 MHz. Two prominent areas of chemical exchange are evident near Cys 14 and Cys 38.

$$\alpha^* = \left(\frac{B_{02} + B_{01}}{B_{02} - B_{01}}\right)\left(\frac{\Delta R_{02} - \Delta R_{01}}{\Delta R_{02} + \Delta R_{01}}\right) \quad (8)$$

in which ΔR_{0i} is the value of ΔR_2 at the *i*th magnetic field strength, B_{0i}. Figure 5 shows ΔR_2 versus the BPTI sequence, and two regions of chemical exchange near Cys 14 and Cys 38 are clearly defined. The scaling factor α^* was calculated using Equation 8 to be 0.6 $\pm$ 0.2 for Cys 38. The value of α for Cys 38 obtained from curve-fitting the full dispersion curve is 0.47 $\pm$ 0.06 (Millet et al., 2000) and agrees well with α^*. Millet and coworkers previously defined an approximate α' using $\Delta R_2' = R_2(1/\tau_{cp} = 15.4\ s^{-1}) - R_2(1/\tau_{cp} = 1000\ s^{-1})$; however, this definition yields much poorer estimates of α because $R_2(1/\tau_{cp} = 1000\ s^{-1})$ is always greater than R_2^0 (Millet et al., 2000). Therefore, ΔR_2 and α^* provide convenient methods for identifying and determining the time scales of chemical exchange processes without acquiring full relaxation dispersion curves.

Although the present results were obtained using a ^{15}N-labeled protein sample, the experiments are facilitated if ^{2}H/^{15}N-labeled samples are utilized. Deuteration reduces ^{1}H-^{1}H dipolar interactions, which reduces relaxation losses during the constant T/2 period (Equation 4) and renders the decay of antiphase magnetization and two spin order less multi-exponential. In addition, both η_z and η_{xy} relaxation interference rate constants can be measured for a ^{2}H/^{15}N-labeled protein, and R_{20}^{rczz} can be obtained without assuming a constant value of the ^{15}N CSA (Kroenke et al., 1998).

In conclusion, the modified relaxation-compensated CPMG pulse sequences for backbone amide ^{15}N spins incorporate a relaxation period for two-spin order that eliminates contributions from proton longitudinal relaxation and enables independent determination of the relaxation rate constant in the limit of fast pulsing. The new CPMG experiments facilitate the characterization of chemical exchange processes, particularly when exchange kinetics are faster than the maximum achievable pulsing rate.

Acknowledgements

This work was supported by National Institutes of Health grant GM59273 awarded to A.G.P.; acquisition of the DRX600 spectrometer was supported by National Science Foundation grant DBI-9601661.

References

Akke, M. and Palmer, A.G. (1996) *J. Am. Chem. Soc.*, **118**, 911–912.
Carver, J.P. and Richards, R.E. (1972) *J. Magn. Reson.*, **6**, 89–105.
Cavanagh, J., Fairbrother, W.J., Palmer, A.G. and Skelton, N.J. (1996) *Protein NMR Spectroscopy*, Academic Press, San Diego, CA.
Delaglio, F., Grzesiek, S., Vuister, G.W., Zhu, G., Pfeifer, J. and Bax, A. (1995) *J. Biomol. NMR*, **6**, 277–293.
Farrow, N.A., Muhandiram, R., U., S.A., Pascal, S.M., Kay, C.M., Gish, G., Shoelson, S.E., Pawson, T., Forman-Kay, J.D. and Kay, L.E. (1994) *Biochemistry* **33**, 5984–6003.
Farrow, N.A., Zhang, O., Szabo, A., Torchia, D.A. and Kay, L.E. (1995) *J. Biomol. NMR*, **6**, 153–162.
Fushman, D., Tjandra, D. and Cowburn, D. (1998) *J. Am. Chem. Soc.*, **120**, 10947–952.
Glushka, J., Lee, M., Coffin, S. and Cowburn, D. (1989) *J. Am. Chem. Soc.*, **111**, 7716–7722.
Huang, K., Andrec, M., Heald, S., Blake, P. and Prestegard, J.H. (1997) *J. Biomol. NMR*, **10**, 45–52.
Ishima, R. and Torchia, D.A. (1999) *J. Biomol. NMR*, **14**, 369–372.
Ishima, R., Wingfield, P.T., Stahl, S.J., Kaufman, J.D. and Torchia, D.A. (1998) *J. Am. Chem. Soc.*, **120**, 10534–10542.
Jen, J. (1978) *J. Magn. Reson.*, **30**, 111–128.
Kroenke, C.D., Loria, J.P., Lee, L.K., Rance, M. and Palmer, A.G. (1998) *J. Am. Chem. Soc.*, **120**, 7905–7915.
Kroenke, C.D., Rance, M. and Palmer, A.G. (1999) *J. Am. Chem. Soc.*, **121**, 10119–10125.
Loria, J.P., Rance, M. and Palmer, A.G. (1999a) *J. Am. Chem. Soc.*, **121**, 2331–2332.
Loria, J.P., Rance, M. and Palmer, A.G. (1999b) *J. Biomol. NMR*, **15**, 151–155.
Luz, Z. and Meiboom, S. (1963) *J. Chem. Phys.*, **39**, 366–370.
Marion, D., Ikura, M., Tschudin, R. and Bax, A. (1989) *J. Magn. Reson.*, **85**, 393–399.
Millet, O., Loria, J.P., Kroenke, C.D., Pons, M. and Palmer, A.G. (2000) *J. Am. Chem. Soc.*, **122**, 2867–2877.
Mulder, F.A.A., Skrynnikov, N.R., Hon, B., Dahlquist, F.W. and Kay, L.E. (2001) *J. Am. Chem. Soc.*, **123**, 967–975.
Otting, G., Liepinsh, E. and Wüthrich, K. (1993) *Biochemistry*, **32**, 3571–3582.
Palmer, A.G., Skelton, N.J., Chazin, W.J., Wright, P.E. and Rance, M. (1992) *Mol. Phys.*, **75**, 699–711.
Phan, I.Q.H., Boyd, J. and Campbell, I.D. (1996) *J. Biomol. NMR*, **8**, 369–378.
Shaka, A.J., Barker, P.B. and Freeman, R. (1985) *J. Magn. Reson.*, **64**, 547–552.
Skrynnikov, N.R., Mulder, F.A.A., Hon, B., Dahlquist, F.W. and Kay, L.E. (2001) *J. Am. Chem. Soc.*, **123**, 4556–4566.
Tjandra, N., Szabo, A. and Bax, A. (1996) *J. Am. Chem. Soc.*, **118**, 6986–6991.